ELSEVIER

Journal of Alloys and Compounds 336 (2002) 18–28

Journal of ALLOYS AND COMPOUNDS

www.elsevier.com/locate/jallcom

Theoretical study of the phase stability and site preference for $R_3(Fe,T)_{29}$ (R=Nd, Sm; T=V, Ti, Cr, Cu, Nb, Mo, Ag)

L.Z. Cao[a,*], J. Shen[a], N.X. Chen[a,b]

[a]*Institute of Applied Physics, Beijing University of Science and Technology, Beijing 100083, PR China*
[b]*Department of Physics, Tsinghua University, Beijing 100084, PR China*

Received 20 June 2001; accepted 10 September 2001

Abstract

The phase stability of intermetallics $R_3(Fe,T)_{29}$ with $Nd_3(Fe,Ti)_{29}$ structure and site preference of some 3d or 4d transition elements T were investigated in molecular static and molecular dynamic methods with a series of ab initio pair potentials obtained though the *lattice inversion method*. Calculated results show that adding either Cr, Mo, Ti, V or Nb atoms makes the crystal cohesive energy of $R_3(Fe,T)_{29}$ decrease markedly, proving that these atoms can stabilize $R_3(Fe,T)_{29}$ with the structure of $Nd_3(Fe,Ti)_{29}$, even though the R_3Fe_{29} crystal structure is itself metastable. The calculated lattice parameters are in good agreement with the experimental data. The degree of the decrease in cohesive energy corresponds with the species and occupation sites of the ternary atoms. The order of site preference of these stabilizing elements T is 4*i*2, 4*i*1 and 4*g* with the occupation of 4*i*2 corresponding to the greatest energy decrease. The calculated result further shows that the addition of Cu or Ag cannot play a role in stabilizing the structure. These calculated results correspond well to available experiments. Supported by the pair potentials, calculated structures are stable within a certain temperature range and the space group of the final structure remains unchanged with respect to a variety of initial deformations. So it was confirmed that there exist a series of $R_3(Fe,T)_{29}$ compounds with the stable structure of $Nd_3(Fe,Ti)_{29}$ in the R–Fe–T systems. The process of the evolution from the RFe_5 structure to metastable R_3Fe_{29} was well explained too with the pair potential in this paper. All these prove the effectiveness of ab initio pair potentials obtained through the *lattice inversion method* in the description of rare-earth materials. © 2002 Elsevier Science B.V. All rights reserved.

Keywords: Rare earth compounds; Transition metal compounds; Crystal structure

1. Introduction

In 1993, the structure of the iron-based compound previously reported as $Nd_2Fe_{19-x}Ti_x$ [1] was first suggested by Cadogan and his colleagues as a $Nd_3(Fe,Ti)_{29}$-type structure (3:29) with monoclinic symmetry. Then Fuerst et al. [2] suggested that the new phase belonged to the *P21/c* space group, which was later confirmed with XRD [3] and neutron powder diffraction [4]. Subsequent work by Kalogirou et al. [5] suggested that the $Nd_3(Fe,Ti)_{29}$-type structure could be described more accurately in the *A2/m* space group than in the *P21/c* space group. Since then, many 3:29 type compounds and their interstitial compounds with the same structure have been discovered [6–8]. It has been found that some interstitial compounds show high Curie temperatures, high magnetic moments and large magneto-crystalline anisotropy, valuable for practical applications [9]. Actually, the binary compound R_3Fe_{29} is metastable [10], but if a certain amount of some ternary elements T (T=Cr, Mo, V, Ti, Nb) is added, $R_3(Fe,T)_{29}$ becomes stable. The crystal cell of R_3Fe_{29} includes two formula units (64 atoms) as shown in Fig. 1. In the *A2/m* space group description, there are 13 crystallographic sites with the rare earth atoms occupying the 2*a* and 4*i* sites, while in the *P21/c* space group description, there are 17 crystal sites, with the rare earth atoms occupying the 2*a* and 4*e* sites. According to the neutron diffraction and X-ray diffraction, most stabilizing elements preferentially replace the Fe atoms, and these preferred Fe sites are 4*i*2, 4*i*1 and 4*g* in the *A2/m* space description [11] and 4*e*3, 4*e*4 and 4*e*14 in the *P21/c* [12] description.

The structure of $R_3(Fe,T)_{29}$ can be regarded as a derivative of the binary structure R_3Fe_{29}. Furthermore, this binary structure can be represented as a derivative of the hypothetical $CaCu_5$ type compound RFe_5, provided that 2/5 of the R atoms are replaced by Fe–Fe dumbbells [13].

*Corresponding author.
E-mail address: lzhcao@sohu.com (L.Z. Cao).

0925-8388/02/$ – see front matter © 2002 Elsevier Science B.V. All rights reserved.
PII: S0925-8388(01)01863-1

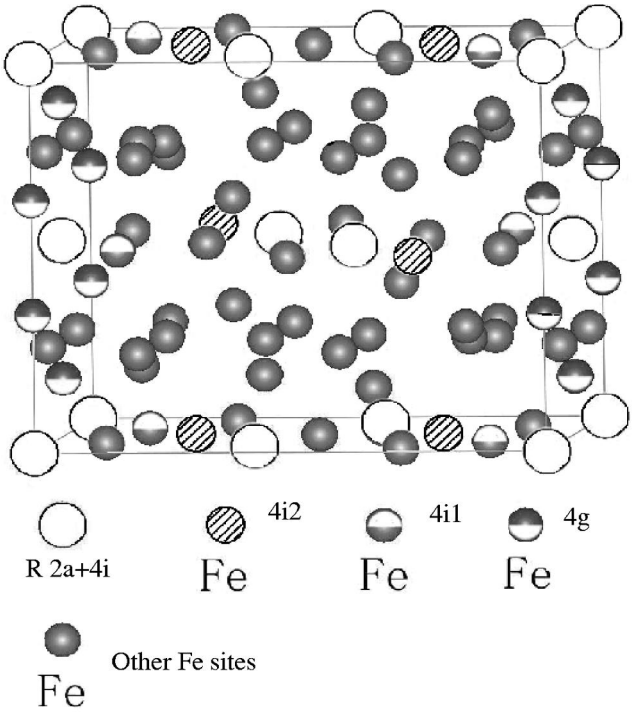

Fig. 1. The crystal cell in the structure of $Nd_3(Fe, Ti)_{29}$ with two R_3Fe_{29} formula units.

The process of evolution from the RFe_5 structure to the metastable R_3Fe_{29}, the stability of $R_3(Fe,T)_{29}$ and the site preferential occupation of T elements in $R_3(Fe,T)_{29}$ were analyzed and evaluated. The pair potentials used here were determined by using a general lattice-inversion technique and a first-principles-based crystal cohesive energy calculation. In one of our previous reports, the pair potentials in $Gd(Fe,T)_{12}$, another series of compounds in the R–Fe–T systems, had been obtained though the same method and applied to the calculation of $Gd(Fe,T)_{12}$ [14]. Compared with the calculation of $Gd(Fe,T)_{12}$, this work is more challenging to the pair potentials used in the calculation since $R_3(Fe,T)_{29}$ materials are much more complex than $Gd(Fe,T)_{12}$ materials.

Chen's lattice inversion method through which we obtained the interatomic pair potentials used in our calculations is briefly introduced in Section 2 of this paper. The calculated results including a description of the process of evolution from the RFe_5 structure to the metastable R_3Fe_{29} are presented in Section 3. A qualitative analysis and a concise discussion about the result follows in Section 4, and the last section contains conclusions.

2. Lattice inversion theorem

In general, any interatomic pair potential can be obtained by strict lattice inversion of the cohesive energy curves, and the cohesive energy curves can be obtained either by first principle calculation or by experimental data fitting. Here we focus on the lattice inversion theorem.

We take a single element crystal as an example to explain how to use Chen's lattice inversion method to obtain the interatomic pair potential based on a first principle cohesive energy curve [15–19].

Suppose that the crystal cohesive energy obtained by the first principle calculation can be expressed as

$$E(x) = \frac{1}{2}\sum_{n=1}^{\infty} r_0(n)\Phi(b_0(n)x) \tag{1}$$

where x is the nearest-neighbor interatomic distance, $r_0(n)$ the nth neighbor coordination number, $b_0(n)x$ the distance between the reference central atom and its nth neighbor, and $\Phi(x)$ is the pair potential. By self-multiplicative process of the element in $\{b_0(n)\}$, the $\{b(n)\}$ forms, a closed multiplicative semi-group. This implies that a large number of virtual lattice points are involved, but the corresponding virtual coordination number is zero. In the $\{b(n)\}$, for two arbitrary integers m and n, there must exist a sole integer k which satisfies $b(k) = b(m)b(n)$. Hence, Eq. (1) can be rewritten as

$$E(x) = \frac{1}{2}\sum_{n=1}^{\infty} r\,(n)\Phi(b(n)x) \tag{2}$$

where

$$r(n) = \begin{cases} r_0\left(b_0^{-1}[b(n)]\right), & \text{if} \quad b(n) \in \{b_0(n)\}, \\ 0 & \text{if} \quad b(n) \notin \{b_0(n)\} \end{cases} \tag{3}$$

Then the general equation for the interatomic pair potential obtained from inversion can be expressed as

$$\Phi(x) = 2\sum_{n=1}^{\infty} I(n)E(b(n)x) \tag{4}$$

the coefficient $I(n)$ can be obtained by

$$\sum_{b(n)1b(k)} I(n)r\left(b^{-1}\left[\frac{b(k)}{b(n)}\right]\right) = \delta_{kl} \tag{5}$$

$I(n)$ is uniquely determined by the crystal geometrical structure, which is independent of the kind of the concrete element. Thus the interatomic pair potentials can be obtained from the known cohesive energy function $E(x)$.

The interatomic pair potential between different kinds of atoms used to study the rare earth intermetallic structures can be obtained by the same inversion method. By a method similar to that applied in our previous work on $Gd(Fe,T)_{12}$, we further obtained the necessary ab initio interatomic pair potentials.

Several important relevant interatomic pair potential curves are shown in Fig. 2, which are close to Morse function, that is

$$\Phi(R) = D_0[u^2 - 2u]$$

with

$$u = e^{[-\frac{\gamma}{2}(\frac{R}{R_0}-1)]},$$

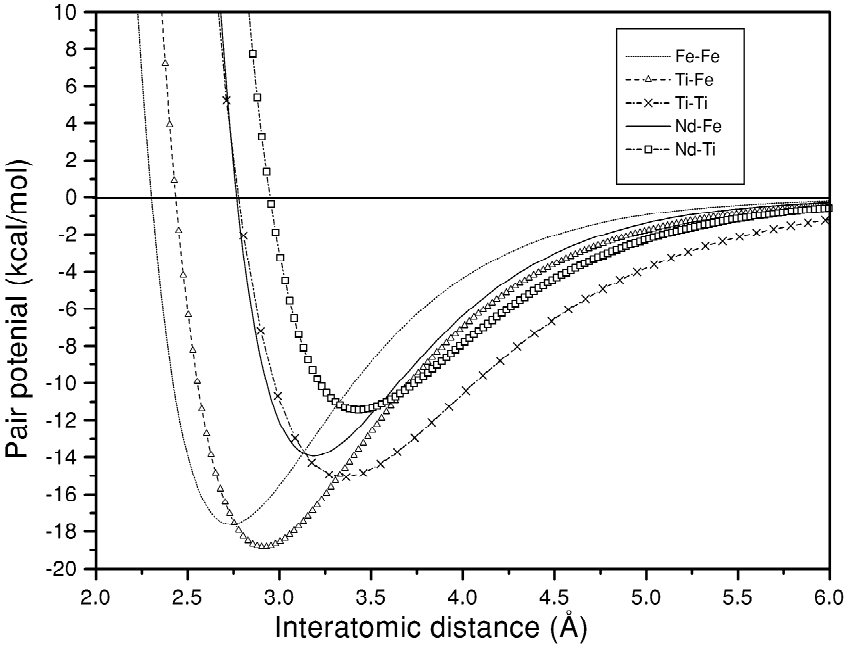

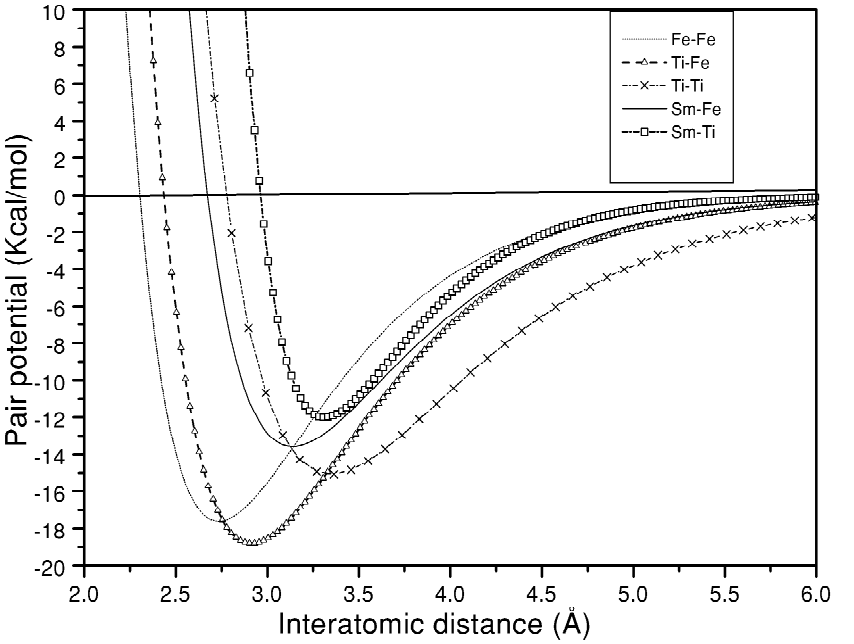

Fig. 2. Some important interatomic potentials.

Table 1
Part of Morse parameters of the conversed pair potentials

Potential types	R_0 (Å)	D_0 (eV)	γ
Sm–Fe	3.1394	0.5891	9.3459
Sm–Ti	3.3115	0.5212	13.1605
Fe–Fe	2.7361	0.7643	8.7529
Fe–Ti	2.9140	0.8166	8.4390
Nd–Fe	3.1889	0.6038	10.4963
Nd–Ti	3.4309	0.4966	9.8818

and part of the Morse parameters acquired from the conversed potentials are listed in Table 1.

3. Results

3.1. The process of evolution from RFe_5 structure to metastable R_3Fe_{29}

It is well-known that the replacement of 2/5 of the Sm

atoms in $SmFe_5$ structure by pairs of iron atoms results in Sm_3Fe_{29}, but a prior exact distribution of those Sm atoms to be replaced by pairs of iron atoms in the $SmFe_5$ structures is unknown. In the simulation process, the change in distribution of the substituted Sm atoms will result in a change of the final Sm_3Fe_{29} structure, though each of them corresponds to the same molecular formula Sm_3Fe_{29}. To solve this problem, we adopt the cohesive energy as a criterium to differentiate between the possible Sm_3Fe_{29} structures from all those R_3Fe_{29} structures obtained via various types of substitutions, and to distinguish between the appropriate types of evolutions. Our calculated result is consistent with the known experiments which show that the most possible Sm_3Fe_{29} structure is the $Nd_3(Fe,Ti)_{29}$ structure with *A2/m* space group. Here we present the simulation process of the phase formation from $SmFe_5$ to Sm_3Fe_{29} with the structure of the known $Nd_3(Fe,Ti)_{29}$. Fig. 3 illustrates the whole simulation process.

A rectangular $SmFe_5$ unit cell is shown in Fig. 3(1). The structure parameters of $SmFe_5$ can be calculated by the conjugate gradient method using ab initio pair potentials $\Phi_{Fe-Fe}(x)$, $\Phi_{Sm-Sm}(x)$ and $\Phi_{Sm-Fe}(x)$ and the calculated results are $a=4.147$ Å and $c=5.034$ Å, which are very close to those obtained from the experiments, $a=4.15$ Å and $c=4.96$ Å [20].

Let the evolution process start from a rectangular $(SmFe_5)_{5\times5\times1}$ supercell (Fig. 3(2)). For each of the five layers along the *X*-axis in the $(SmFe_5)_{5\times5\times1}$ supercell, choose 2/5 of the Sm (Fig. 3(2)) and replace each of them by a pair of Fe atoms mutually separated by a 0.1 Å space and having random orientation, in this way $R_{30}Fe_{290}$ is obtained (Fig. 3(3)). Once the ab initio pair potentials are taken into account, the orientation and the length of the dumbbells change immediately, and at the same time the site distribution of all the atoms is rearranged, and the lattice constants are adjusted. The final structure was determined to have the structure parameters $a=10.5818$ Å, $b=8.4875$ Å, $c=9.7241$ Å, $\beta=97.0732°$ and the length of the dumbbells is 2.449 Å, as shown in Fig. 3(4). The unit cell of this final structure is shown in Fig. 3(5), from which one can see that it is the same structure as the

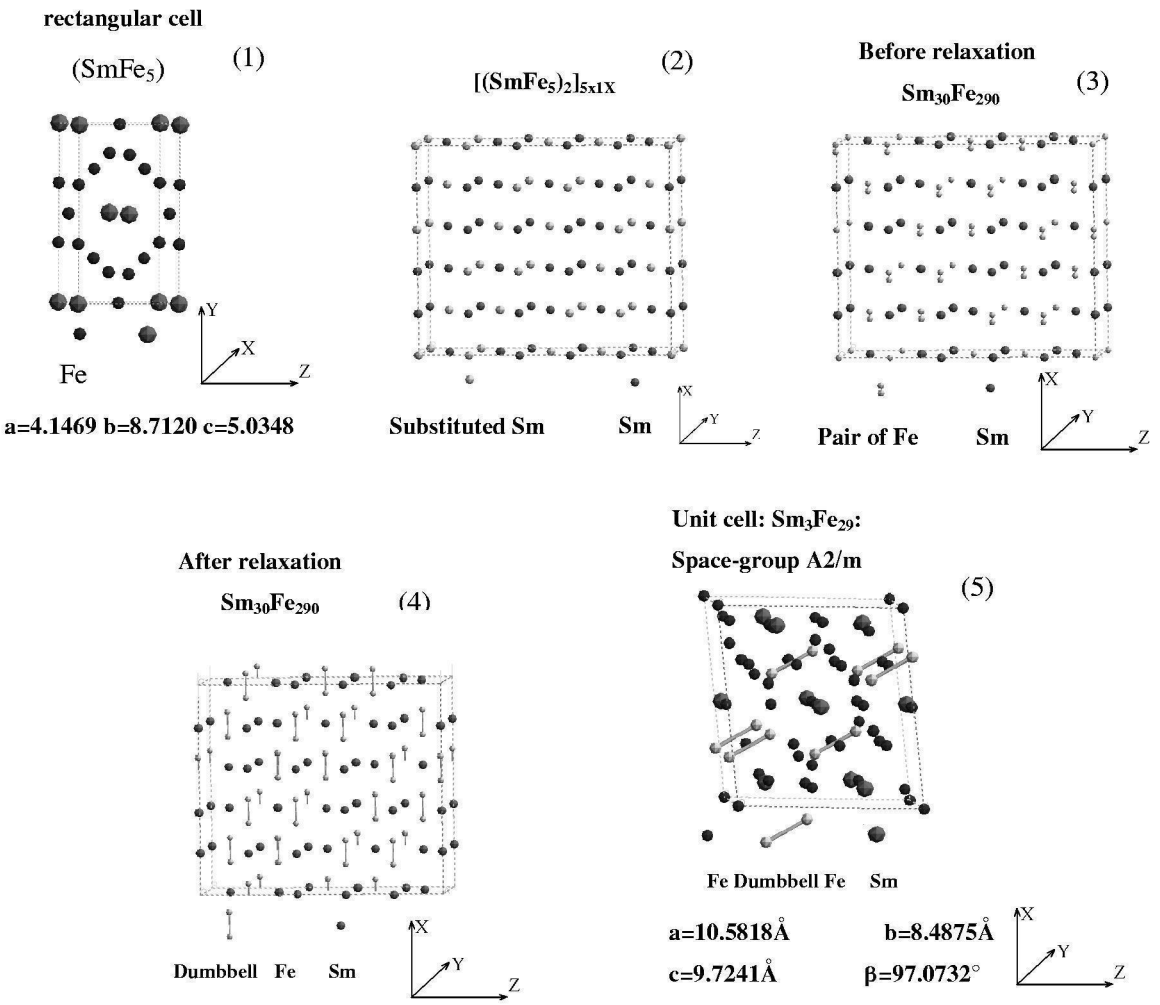

Fig. 3. The process of evolution from the $SmFe_5$ structure to metastable Sm_3Fe_{29} with the structure of $Nd_3(Fe,Ti)_{29}$. *To show the process more clearly, only the Sm atoms replaced by dumb-bell Fe atoms and the corresponding dumb-bell Fe atoms are visible in (2), (3) and (4) in this figure.

$Nd_3(Fe,Ti)_{29}$-type structure found in experiments with *A2/m* space. We can also learn from this process that, of the three Fe sites 4*i*1, 4*i*2 and 4*g* preferred by the ternary elements, the 4*i*1 and 4*i*2 sites are among the dumb-bell Fe sites. Thus, the evolution process from the $SmFe_5$ structure to Sm_3Fe_{29} with $Nd_3(Fe,Ti)_{29}$ structure is clearly revealed. The evolution process of Nd_3Fe_{29} is similar to that of Sm_3Fe_{29}.

3.2. Calculated results for binary R_3Fe_{29}

Although the structure of R_3Fe_{29} is metastable, it can be considered as the proto-type of $Nd_3(Fe,Ti)_{29}$-type structure. It is worth mentioning that, in the calculation, once the energy minimization based on ab initio *atomistic pair potentials* is carried out, the somehow arbitrary initial lattice structure will be stabilized to a structure close to the existing $Nd_3(Fe,Ti)_{29}$ structure, provided that the initial model does not deviate too much from the existing $Nd_3(Fe,Ti)_{29}$ structure. The lattice constants of the initial model and final model are listed in Table 2. The randomness of the initial structure in a certain range and the stability of the final structure illustrate that R_3Fe_{29} has the topological invariability with respect to the existing $Nd_3(Fe,Ti)_{29}$ structure. Hence it furnishes convincing evidence that the interatomic pair potentials are reliable for the study of structural material characteristics.

3.3. The phase stability of $R_3(Fe,T)_{29}$

In the course of the calculation, we took 14 Å as the cut-off radius. Energy minimization was carried out with the conjugate gradient method. In order to reduce statistical fluctuations, we took the periodical cell containing 512 atoms $(R_3Fe_{29-x}T_x)_{16}$, as a calculation unit.

The relation between the crystal cohesive energy and the stabalizing elements content are shown in Fig. 4. It can be seen that for T=Cr, Mo, Ti, V or Nb the cohesive energy decreases with the ternary elements content, illustrating that each of these elements can stabilize the crystal structure and correspondingly the stabilized phases exist, but for T=Cu or Ag, the cohesive energy of $R_3(Fe,T)_{29}$ increases, which means that these ternary elements cannot stabilize the R_3Fe_{29} system with the structure of $Nd_3(Fe,Ti)_{29}$. (The total energies of the intermetallics shown in the figure are the statistical average of 100 calculation examples, the error bars indicate the range of mean square root error).

The calculated lattice constants were compared with the experimental values, as shown in Table 3. From the table, one can see not only the agreement of the calculated lattice constants with the experimental values, but also the tendency of lanthanide contraction from Nd to Sm.

The structure calculations of $Sm_3Fe_{27.5}Ti_{1.5}$ and $Nd_3Fe_{27.5}Ti_{1.5}$ retain *A2/m* within a tolerance range of 0.321–1.00 Å for the former and 0.182–1.00 Å for the latter. To check the stability of the calculation structures, we allowed every atom in the $R_3Fe_{27.5}Ti_{1.5}$ crystal cell to randomly move 0.7 Å in arbitrary directions. Then we used the conjugate gradient for energy minimization. The results show that the lattice constants of the final structure are still retained in good agreement with the experimental data, as shown in Table 4. The tolerance for the *A2/m* structure increases slightly with increasing atomic motion range, and once the range exceeds 0.7 Å, the space symmetry of the system drops largely (Table 5).

3.4. Site preference substitution of T atoms in $R_3(Fe,T)_{29}$

According to known experiments, ternary elements prefer to occupy three Fe sites, 4*i*2, 4*i*1 and 4*g*. The average cohesive energy when ternary elements randomly occupy one or more of 4*i*2, 4*i*1 and 4*g* sites was compared with that when the ternary elements randomly occupy other Fe sites in the structure. (Only examples with cells that could retain the *A2/m* space group within a tolerance of 0.5 Å after relaxation were counted.) The number of the calculated examples was 300. As is shown in Table 6, the average energy of the former case is lower than the latter. Therefore, the calculated results are consistent with the experimental conclusion that, although the ternary elements can be found in all the Fe sites, they prefer to occupy the 4*i*2, 4*i*2, 4*g* sites. It should be noted that

Table 2
Final crystal lattice constants of R_3Fe_{29} (R=Nd, Sm) corresponding to random initial structures

a (Å)	*b* (Å)	*c* (Å)	*α*	*β*	*γ*	*a* (Å)	*b* (Å)	*c* (Å)	*α*	*β*	*γ*
Initial state (R=Sm)						Final state (R=Sm)					
15	18	14	70	80	70	10.582	8.488	9.724	90	97.07	90
20	20	20	90	120	90	10.582	8.487	9.724	90	97.08	90
8	5	3	60	70	80	10.582	8.488	9.724	90	97.08	90
3	3	3	90	60	90	10.579	8.488	9.725	90	97.06	90
Initial state (R=Nd)						Final state (R=Nd)					
15	18	14	70	80	70	10.671	8.554	9.774	90	97.22	90
20	20	20	90	120	90	10.671	8.554	9.774	90	97.22	90
8	5	3	60	70	80	10.672	8.554	9.774	89.99	97.23	89.99
3	3	3	90	60	90	10.671	8.553	9.773	90	97.21	90

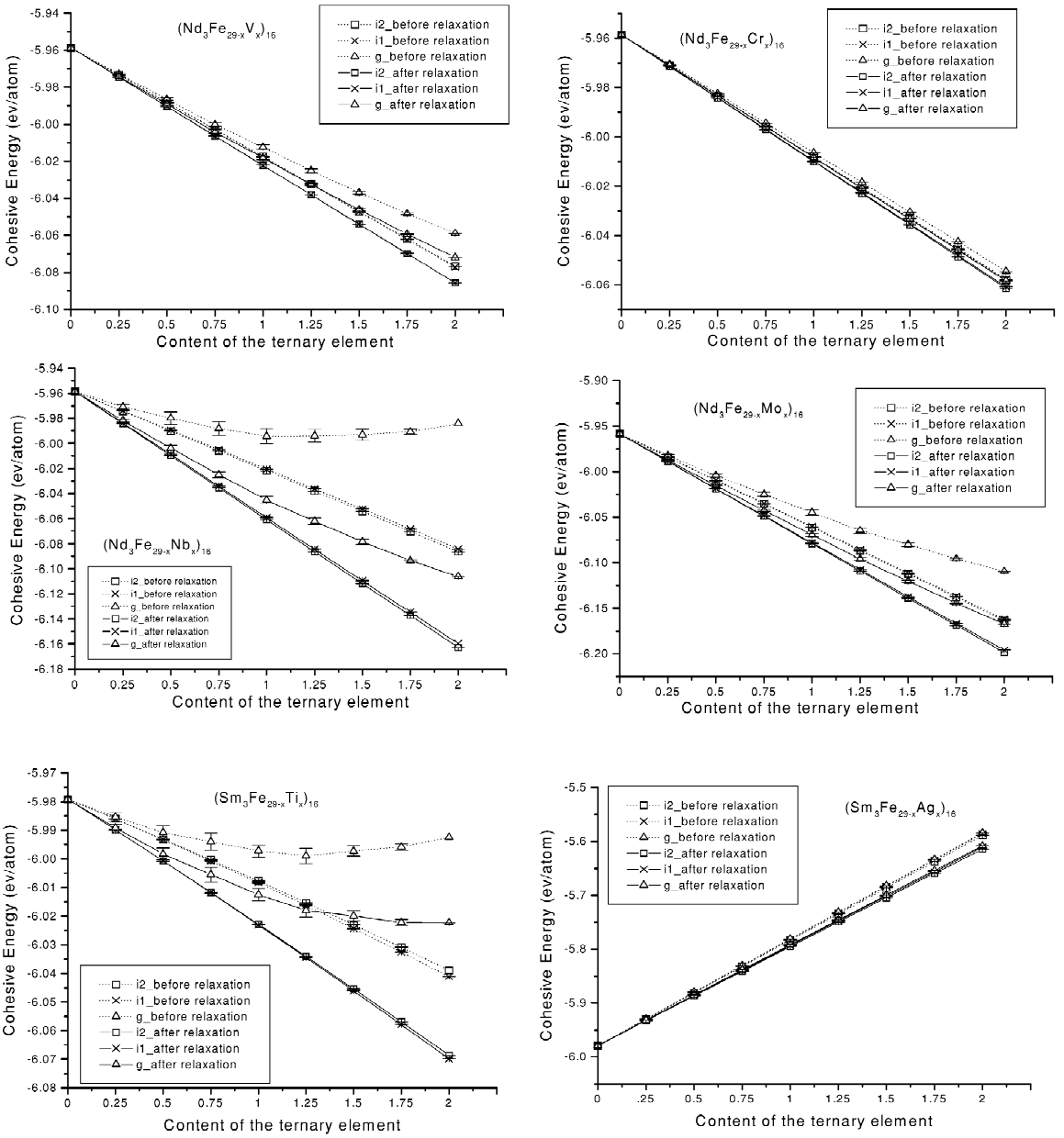

Fig. 4. Site preference and phase stability of $R_3(Fe,T)_{29}$ (T = Cr, V, Mo, Nb, Ti and Ag).

Table 3
Comparison of calculated constants with the experimental data [6,8,21–23]

	Cal. *a* (Å)	Exp. *a* (Å)	Cal. *b* (Å)	Exp. *b* (Å)	Cal. *c* (Å)	Exp. *c* (Å)	Cal β (°)	Exp. β (°)
$Sm_3Fe_{26.75}V_{2.25}$	10.628	10.605	8.549	8.546	9.752	9.708	97.14	96.86
$Sm_3Fe_{27}Ti_2$	10.645	10.620	8.564	8.56	9.796	9.720	96.93	96.97
$Sm_3Fe_{24}Cr_5$	10.616	10.585	8.541	8.521	9.757	9.684	96.99	96.90
$Sm_3Fe_{28}Mo$	10.617	10.628	8.534	8.566	9.746	9.735	97.14	96.88
$Nd_3Fe_{27}V_2$	10.705	10.647	8.597	8.574	9.791	9.738	97.31	96.85
$Nd_3Fe_{27.5}Ti_{1.5}$	10.711	10.660	8.601	8.595	9.813	9.751	97.18	96.77
$Nd_3Fe_{24.5}Cr_{4.5}$	10.704	10.615	8.592	8.556	9.793	9.714	97.24	96.90
$Nd_3Fe_{27.75}Mo_{1.25}$	10.710	10.642	8.604	8.583	9.802	9.748	97.27	96.88

Table 4
The comparison of related lattice constants before and after atomic random motion of 0.7 Å for $Sm_3Fe_{27.5}Ti_{1.5}$ and $Nd_3Fe_{27.5}Ti_{1.5}$

	$Sm_3Fe_{27.5}Ti_{1.5}$				$Nd_3Fe_{27.5}Ti_{1.5}$			
	a	*b*	*c*	*β*	*a*	*b*	*c*	*β*
Before random motion	10.6648	8.5641	9.7757	96.8378	10.7166	8.6000	9.8125	97.1458
After random motion of 0.7 Å	10.6647	8.5639	9.7758	96.8399	10.7166	8.6000	9.8125	97.1456
Exp.	10.62	8.56	9.72	96.972	10.660	8.595	9.751	96.771

cohesive energy difference is relatively large for T=Nb, indicating that a large solubility of Nb in $Nd_3(Fe,Ti)_{29}$-type structure is impossible. Since the stabilizing elements prefer to occupy the 4*i*2, 4*i*1 and 4*g* sites, we will focus on these sites in the following discussion.

It can be seen from Fig. 4 that the calculated cohesive energy decreases most significantly when the T atoms occupy the 4*i*2 site (4*e*3 site in *p21*/*c*), less significantly when the T atoms occupy the 4*i*1 site (4*e*4 in *p21*/*c*), and much more slowly when they occupy the 4*g* site (4*e*14 in *p21*/*c*). Therefore, the T atoms will preferentially occupy 4*i*2 sites. This is also in good agreement with experiments [6,8,21–23]. But from the results of our calculation, one can see that the difference between the decrease for the 4*i*2 site and that for the 4*i*1 site is so small that it can be neglected. So T atoms will preferentially and simultaneously occupy the 4*i*1 site and the 4*i*2 site. This is at variance with some experiments [12] where it was found that 4*i*2(4*e*3) site has much priority over 4*i*1(4*e*4) site.

As shown in Fig. 5, the addition of the T atoms makes the cell expand. It can also be seen that the cohesive energy difference before and after the relaxation, the

Table 5
After the atomic random motion, the relation between the tolerance and the space group of $R_3(Fe,Ti)_{29}$

Range of motion	$Sm_3Fe_{27.5}Ti_{1.5}$		$Nd_3Fe_{27.5}Ti_{1.5}$	
	Tolerance range	Space group	Tolerance range	Space group
0.1 Å	0.001–0.258	*Pm*	(0.001–0.002)	*P1*
			(0.003–0.166)	*Pm*
	0.259–0.320	*P2*/*m*	(0.167–0.181)	*P2*/*m*
	0.321–0.5	*A2*/*m*	(0.182–0.5)	*A2*/*m*
0.2 Å	0.001	*P1*	0.001	*P1*
	0.002–0.259	*Pm*	(0.002–0.165)	*Pm*
	0.26–0.322	*P2*/*m*	(0.166–0.180)	*P2*/*m*
	0.323–0.5	*A2*/*m*	0.181–0.5	*A2*/*m*
0.3 Å	0.001	*P1*	0.001	*P1*
	0.002–0.259	*Pm*	(0.002–0.166)	*Pm*
	0.260–0.322	*P2*/*m*	(0.167–0.181)	*P2*/*m*
	0.323–0.5	*A2*/*m*	(0.182–0.5)	*A2*/*m*
0.4 Å	0.001	*P1*	0.001	*P1*
	0.002–0.260	*Pm*	(0.002–0.166)	*Pm*
	0.261–0.322	*P2*/*m*	(0.167–0.181)	*P2*/*m*
	0.323–0.5	*A2*/*m*	(0.182–0.5)	*A2*/*m*
0.5 Å	0.001	*P1*	0.001	*P1*
	0.002–0.258	*Pm*	(0.002–0.165)	*Pm*
	0.259–0.320	*P2*/*m*	(0.166–0.180)	*P2*/*m*
	0.321–0.5	*A2*/*m*	0.182	*A2*/*m*
0.6 Å	0.001	*P1*	(0.001–0.166)	*P1*
	0.002–0.258	*Pm*	(0.167–0.181)	*P2*/*m*
	0.259–0.320	*P2*/*m*	(0.182–0.5)	*A2*/*m*
	0.321–0.5	*A2*/*m*		
0.7 Å	0.001	*P1*	0.001	*P1*
	0.002–0.258	*Pm*	(0.002–0.166)	*Pm*
	0.259–0.321	*P2*/*m*	(0.167–0.181)	*P2*/*m*
	0.322–0.5	*A2*/*m*	(0.182–0.5)	*A2*/*m*
0.8 Å	0.001–1	*P1*	0.001–1	*P1*

The calculated values in Tables 5 and 6 are statistical results of a few calculation examples.

Table 6
Difference in cohesive energy when T atoms randomly occupy Fe sites of the type 4*i*1, 4*i*2 and 4*g* and when T atoms randomly occupy other Fe sites

$R_3Fe_{29-x}T_x$	Diff. for $x=1$ (eV/atom)	Diff. for $x=2$ (eV/atom)	Diff. for $x=3$ (eV/atom)	Diff. for $x=4$ (eV/atom)
Nd/V	0.0095	0.0191	0.0291	0.0352
Nd/Ti	0.0101	0.0196	0.0257	0.0284
Nd/Cr	0.0088	0.0169	0.0264	0.0345
Nd/Mo	0.0162	0.0304	0.0352	0.0515
Nd/Nb	0.0158	0.0314	0.0387	0.0491
Sm/V	0.0074	0.0135	0.0223	0.0264
Sm/Ti	0.0081	0.0129	0.0122	0.0162
Sm/Cr	0.0095	0.0183	0.0271	0.0372
Sm/Mo	0.0163	0.0257	0.0372	0.0481
Nd/Nb	0.01961	0.02281	–	–

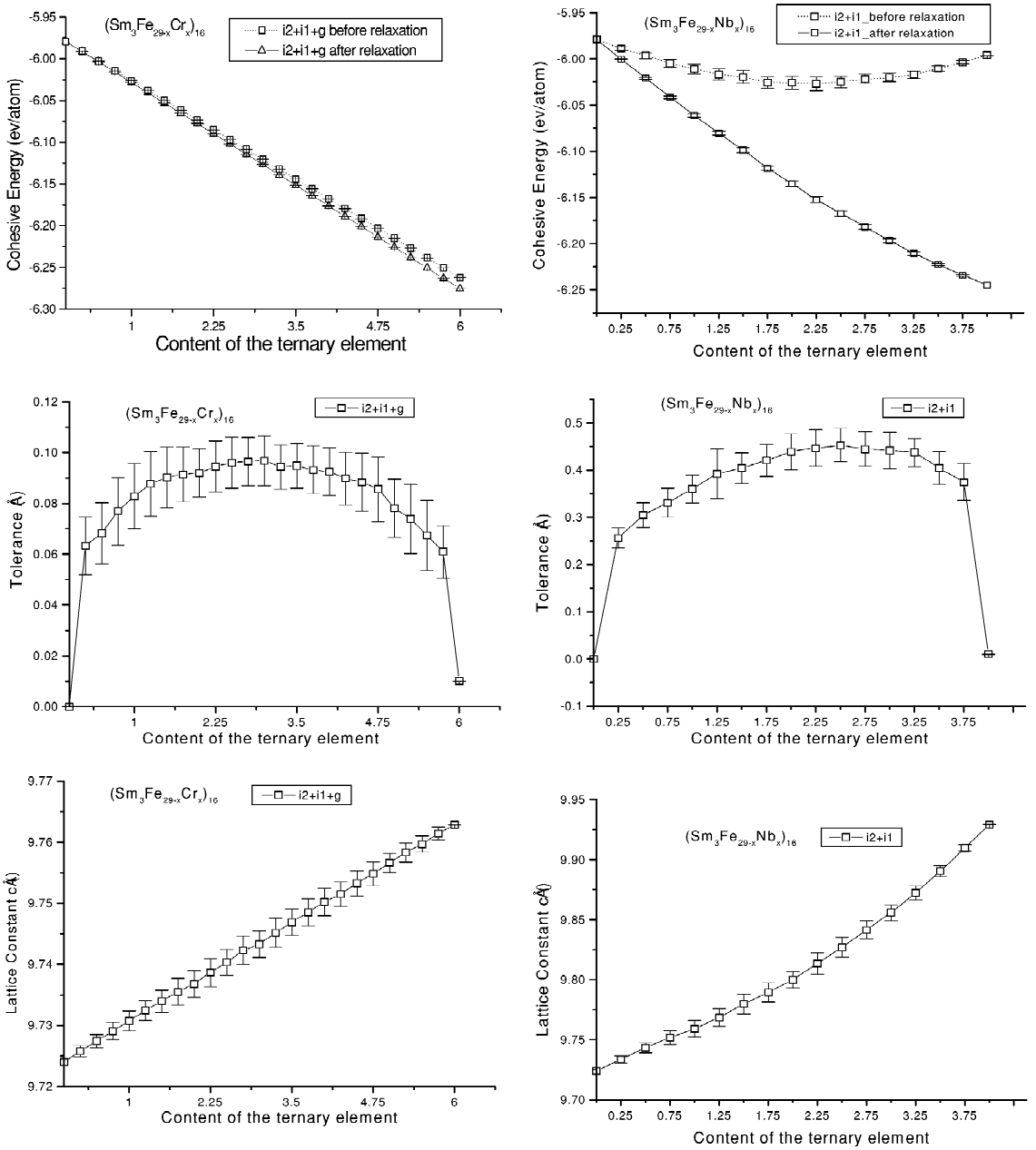

Fig. 5. Comparison of the changes of cohesive energy, tolerance and lattice constants for $Sm_3Fe_{29-x}Cr_x$ and $Sm_3Fe_{29-x}Nb_x$ after relaxation.

Table 7
The relationship between the tolerance and space group of $Nd_3Fe_{27.5}Ti_{1.5}$ and $Sm_3Fe_{27}Ti_2$ in MD

R	T (K)	Crystal constants				Tolerance range (Å)	Space group
		a (Å)	b (Å)	c (Å)	$\beta°$		
Nd	300	10.7302	8.6152	9.8453	97.4105	0.4–	*A2/m*
	500	10.6779	8.6401	9.9548	97.2995	0.43–	*A2/m*
	700	10.7622	8.6291	9.932	97.5875	0.43–	*A2/m*
	900	10.693	8.6559	9.8028	97.11	0.45–	*A2/m*
	1200	10.9001	8.6580	9.7959	98.0585	0.5–	*A2/m*
Sm	300	10.7849	8.5291	9.7593	96.7113	0.38–	*A2/m*
	500	10.7929	8.579	9.7961	96.7085	0.38–	*A2/m*
	700	10.638	8.6021	9.8679	96.7305	0.38–	*A2/m*
	900	10.5582	8.6703	9.8371	96.5481	0.5–	*A2/m*
	1200	10.6602	8.6543	9.9618	96.5885	0.58–	*A2/m*

tolerance and the change of lattice constants are relatively small for T = Cr, and relatively large for T = Nb. Since the dependence of lattice constants and the tolerance on the content of ternary element can, to some extent, reflect information on structural changes, these results could mean that the solubility of Cr is higher than that of Nb. In this way, we obtain a rough solubility sequence of the ternary elements in the structure of $Nd_3(Fe,Ti)_{29}$, from the largest to the smallest: Cr, V, Ti, Mo, and Nb. This conclusion is in good agreement with known experimental results [6,8,21–23]. The number of calculated examples here is 300.

3.5. Molecular dynamic calculation for $R_3(Fe,Ti)_{29}$

The stability of the calculated structure was further checked through molecular dynamics. The relation between the tolerance and space group is traced to higher temperatures, as shown in Table 7. Using MD (molecular dynamics) NPT ensemble, with $P = 1$ atm, $t = 0.001$ ps, dynamic simulations for $(Sm_3Fe_{27}Ti_2)_{16}$ and $(Nd_3Fe_{27.5}Ti_{1.5})_{16}$ were carried out at temperatures of 300, 500, 700, 900 and 1200 K. The symmetry could also remain *A2/m* in a certain range of tolerance, and the lattice constants changed very little with respect to temperature variation. Thus the structural stability was again verified. These results further verify that the above calculations are self-consistent and reasonable.

The comparisons of potential energy, kinetic energy and the fluctuations at different temperatures are shown in Table 8. It can be seen that the potential energy and kinetic energy as well as the fluctuations all increase with the increase of temperature. Compared with the absolute potential energy values, the fluctuations are small. Therefore the crystal structure at different temperatures is basically determined by the interatomic pair potentials.

4. Discussion

4.1. Phase stability

What follows is an analysis in terms of interatomic pair potential. When a certain amount of the ternary element atoms substitute for Fe atoms, the ternary element atom is surrounded most by Fe atoms. The Nd or Sm atoms are not their own nearest neighbor atoms, and the occasions on which T atoms are their own nearest neighbors are truly rare. Therefore, the pair potential of $\Phi_{T-T}(r)$ has less influence on the structure stability due to the substitution behavior and can be ignored. The energy difference caused by the substitution is mainly determined by the difference between $\Phi_{Fe-T}(r)$ and $\Phi_{Fe-Fe}(r)$. If $\Phi_{Fe-T}(r) < \Phi_{Fe-Fe}(r)$, T elements can stabilize the structure. On the contrary, if $\Phi_{Fe-T}(r) > \Phi_{Fe-Fe}(r)$, then T elements cannot play the role of stabilization. This can explain why elements belonging to the family V, Ti, Cr, Mo, Nb stabilize the structure, while Cu and Ag do not.

When the amount of ternary element atoms increases, the possibility that T atoms are close to T atoms or to rare earth atoms increases. Then the comparison between

Table 8
The potential and kinetic energies and their fluctuations

T (K)	$Sm_3Fe_{27}Ti_2$					$Nd_3Fe_{27.5}Ti_{1.5}$				
	300	500	700	900	1200	300	500	700	900	1200
E_p	−6.011	−6.002	−5.957	−5.929	−5.887	−5.988	−5.961	−5.933	−5.907	−5.864
(eV/atom)	(0.027)	(0.038)	(0.062)	(0.080)	(0.085)	(0.031)	(0.046)	(0.066)	(0.073)	(0.107)
E_K	0.038	0.063	0.089	0.114	0.152	0.038	0.063	0.089	0.113	0.151
(eV/atom)	(0.027)	(0.039)	(0.060)	(0.080)	(0.087)	(0.031)	(0.045)	(0.066)	(0.075)	(0.108)

Shown in parentheses are the energy fluctuations at difference temperatures.

$[\Phi_{R-Fe}(r)-\Phi_{R-T}(r)]$ and $[\Phi_{Fe-Fe}(r)-\Phi_{T-T}(r)]$ has to be made. We can choose T=Ti as an example. From Fig. 2, one can see that the potential values are most important when the distance is less than 4.4 Å. It is also noted that $\Phi_{Fe-Fe}(r)<\Phi_{Ti-Ti}(r)$ within the range of $r<3.1$ Å and $\Phi_{R-Fe}(r)<\Phi_{R-Ti}(r)$ within the range of $r<3.6$ Å. This means that substitution of a large amount of the ternary element may cause the total energy to increase thereby causing structural instability. Hence, the solubility of the ternary element will be limited.

The above analysis explains why some elements can stabilize the binary structure and some do not. Yet in the practical calculation, all of the interatomic pair potentials $\Phi_{Fe-Fe}(r)$, $\Phi_{R-Fe}(r)$, $\Phi_{R-R}(r)$, $\Phi_{R-T}(r)$, $\Phi_{Fe-T}(r)$, $\Phi_{T-T}(r)$ were considered.

4.2. Site preference substitution

The site preference of the stabilizing atoms can also be simply explained by carrying out a cluster analysis of the surroundings of all the Fe sites in the $R_3(Fe,T)_{29}$ crystal based on the comparison of interatomic pair potentials. Since all interatomic distances are larger than 2.3 Å, and the potential values are most important when the distance is less than 4.4 Å, the radius of the cluster is taken as 4.4 Å. Focusing on the range of 2.3 Å$<r<$4.4 Å, one can notice that $\Phi_{Fe-Ti}(r)$ intercepts with $\Phi_{Fe-Fe}(r)$ at about $r=2.7$ Å. When the interatomic distance $r<2.7$ Å, $\Phi_{Fe-Ti}(r)>\Phi_{Fe-Fe}(r)$, which is unfavorable for the substitution of Ti atoms for Fe atoms. When the distance $r>2.7$ Å, $\Phi_{Fe-Ti}(r)<\Phi_{Fe-Fe}(r)$, it is favorable for the substitution. On the other hand, the curve $\Phi_{Nd-Ti}(r)$ intersects the $\Phi_{Nd-Fe}(r)$ curve at approximately $r=3.6$ Å, while the curve $\Phi_{Sm-Ti}(r)$ is always higher than the $\Phi_{Sm-Fe}(r)$ curve within 4.4 Å. Since there is no neighboring Nd or neighboring Sm atom to any Fe atom of any Fe site in the sphere of 3.6 Å$<r<$4.4 Å, what matters is the case of $r<3.6$ Å where $\Phi_{R-Ti}(r)>\Phi_{R-Fe}(r)$, and it is not beneficial to substitute Ti for Fe.

Based on the above potential analysis, the site preference order for substituting T can be qualitatively estimated by accounting for the number of the benefit factors related to in Table 9.

Column 1 in Table 9 includes the Fe sites supposed to be occupied by T atoms. Column 2 shows the number of Fe atoms inside a sphere centered around a T atom with a sphere radius of 2.7 Å. Column 3 corresponds to the number inside the shell from $r_1=2.7$ Å to $r_2=4.4$ Å. Similarly, the fourth and the fifth columns correspond to center atoms being Nd or Sm. The total benefit factors are counted in the last column. When counted in the last column, whether a value from a column before should be positive or negative depends on whether the case of that column is beneficial to the energy decrease after substitution. For example, in the case of column 2 ($r<2.7$ Å), $\Phi_{Fe-T}(r)>\Phi_{Fe-Fe}(r)$ when Fe atoms are replaced by Ti atoms, the more neighboring Fe atoms in this range, the more unfavorable for the energy decrease after substitution, so the values in column 2 are negative. From Table 9, it is easy to reach the conclusion that the ternary elements will preferentially occupy 4*i*2, 4*i*1, and 4*g* Fe sites, and the preferential occupation sequence for the three sites is 4*i*2, 4*i*1, 4*g*.

5. Conclusion

The ab initio interatomic potentials obtained through the lattice inversion method are successfully used to explain the process of evolution from the RFe_5 structure to metastable R_3Fe_{29}. They were used for the calculation of phase stability of $R_3(Fe_{29},T)_{29}$, site preference of T in $R_3(Fe_{29},T)_{29}$ (R=Nd or Sm; T=V, Ti, Cr, Mo, Nb, Cu and Ag) and related parameters. The calculated results are in unexpectedly good agreement with the experimental data and could be well explained with pair potentials.

Despite the randomness of the initial binary R_3Fe_{29} structure and the overall structure deformation as well as the random atomic motion within 0.7 Å for the ternary $R_3(Fe,T)_{29}$ structure, the calculated structure supported by interatomic pair potentials can finally correspond to the existing stable $R_3(Fe,T)_{29}$ structure. The stability of the structure is further confirmed through molecular dynamic simulations at different temperatures. These facts verify that the interatomic pair potentials based on the lattice inversion method can effectively give a deeper insight into the structure and property of complex materials.

Although the binary R_3Fe_{29} compound had been predicted long before, it is still not found yet in experiment. It is difficult to determine the space group of this complex structure in an experimental way since the ternary element play some sophisticated role and the solution to the inverse diffraction spectrum problem cannot distinguish the tiny

Table 9
Benefit factors for distinct Fe sites

Site	No. of Fe ($r<2.7$ Å)	No. of Fe (2.7 Å$<r<$4.4 Å)	No. of (Sm or Nd) ($r<3.6$ Å)	No. of (Sm or Nd) (3.6$<r<$4.4 Å)	Benefit factors
4*i*2	5	26	1	0	$-5+26-1=+20$
4*i*1	6	25	1	0	$-6+25-1=+18$
4*g*	7	22	1	0	$-7+22-1=+14$
Others	7–11	10–19	2–3	0	$-3-+11$

difference between the space groups *A2/m* and *P21/c* for $R_3(Fe,T)_{29}$, while calculations can reveal the change of space group index with respect to the element types and the content of those ternary additions. The computational investigation from the view point of energy also features in dealing with metastable problems. Encouraged by the previous work on $Gd(Fe,T)_{12}$ and the work on $R_3(Fe,T)_{29}$ here, we are confident in future work on material structure research and prediction. As a last point, it should be mentioned that current work does not include many-body interaction and magnetic effect, and that might be the next objective of our work.

Acknowledgements

The authors would like to acknowledge the stimulating discussion with Professor F.M. Yang at Institute of Physics, Chinese Academy of Science. This work is supported partly by the National Advanced Materials Committee in China, partly by the National Foundation of Sciences in China.

References

[1] S.J. Collotcott, R.K. Day, J.B. Dunlop, R.L. Davis, in: Proceedings of the 7th international Symposium on Magnetic Anisotropy and Coercivity in R-T alloys, Canberra, July, 1992, p. 437.
[2] C.D. Fuerst, F.E. Pinkerton, J.F. Herbst, J. Magn. Magn. Mater. 129 (1994) L115.
[3] J.M. Cadogan, H.S. Li, R.L. Davis, A. Margarian, S.J. Collocott, J.B. Dunlop, P.B. Gwan, J. Appl. Phys. 75 (1994) 7114.
[4] Z. Hu, W.B. Yelon, J. Appl. Phys. 76 (1994) 6147.
[5] O. Kalogirou, V. Psycharis, L. Saettas, D.N. Niarchos, J. Magn. Magn. Mater. 146 (1995) 335.
[6] X.F. Han, F.M. Yang, H.G. Pan, Y.G. Wang, J.L. Wang, H.L. Liu, N. Tang, R.W. Zhao, J. Appl. Phys. 81 (11) (1997) 7450.
[7] G.Y. Huo, Z.Y. Qiao, G.H. Rao, X.L. Chen, J.K. Liang, F. Huang, J. Alloys Comp. 283 (1999) 203–207.
[8] H.G. Pan, F.M. Yang, C.P. Chen, X.F. Han, N. Tang, J.F. Hu, J.L. Wang, R.W. Zhao, K.W. Zhou, Q.D. Wang, J. Magn. Magn. Mater. 159 (1996) 352–356.
[9] X.F. Han, R.G. Xu, X.H. Wang, H.G. Pan, E. Baggio-Saitovitch, T. Miyazaki, F.M. Yang, C.P. Chena, J. Magn. Magn. Mater. 190 (1998) 257–266.
[10] A. Margarian, J.B. Dulop, R.K. Day, W. Kalceff, J. Appl. Phys. 76 (10) (1994) 6153–6155.
[11] H. Pan, Y. Chen, X. Han, C. Chen, F. Yang, J. Magn. Magn. Mater. 185 (1998) 77–84.
[12] Z. Hu, W.B. Yelon, Solid State Commun. 91 (3) (1994) 223–226.
[13] C.D. Fuerst, F.E. Pinkerton, J.F. Herbst, J. Appl. Phys. 76 (1994) 6144.
[14] N.X. Chen, J. Shen, X.P. Su, J. Phys.: Condensed Matter 13 (2001) 2727–2736.
[15] N.X. Chen, Z.D. Chen, Y.C. Wei, Phys. Rev. E55 (1997) R5.
[16] N.X. Chen, G.B. Ren, Phys. Rev. B45 (1992) 8177.
[17] N.X. Chen, X.J. Ge, W.Q. Zhang, F.W. Zhu, Phys. Rev. B57 (1998) 14203.
[18] J. Maddox, Nature 344 (1990) 377.
[19] W.Q. Zhang, Q. Xie, X.J. Ge, N.X. Chen, J. Appl. Phys. 82 (2) (1997) 578.
[20] P. Villars, in: Pearson's Handbook Desk Edition, Crystallographic Data for Intermetallic Phases, Vol. 2, ASM International, Materials Park, OH 44073, 1997, p. 1825, CrSi-Zr.
[21] W.A. Mendoza, S.A. Shaheen, J. Magn. Magn. Mater. 195 (1999) 136–140.
[22] A. Margarian, J.B. Dunlop, S.J. Collocott, H.-S. Li, J.M. Cadogan, R.L. Davis, in: Proc. 8th Int. Symp. on Magnetic Anisotropy and Coercivity in R-T Alloys, Birmingham, 1994.
[23] F.M. Yang, B. Nasunjilegal, H.Y. Pan, J.L. Wang, R.W. Zhao, B.P. Hu, Y.Z. Wang, H.S. Li, J.M. Cadogan, J. Magn. Magn. Mater. 135 (1994) 298–302.